# Modeling and Analysis of Nonlinear Sleeve Joints of Large Space Structures

Aldo A. Ferri*
*Georgia Institute of Technology, Atlanta, Georgia*

**A nonlinear sleeve joint model that accounts for the presence of clearances, impact damping, and dry (Coulombic) friction is developed. By studying the free and forced response of this model, it is seen that the overall damping appears to be predominantly viscous-like in nature. This is found to be true even for the cases studied in which dry friction is the sole source of energy dissipation. In addition, the nonlinear behavior of a rigid beam inserted into a sleeve joint is investigated and discussed.**

## I. Introduction

RECENT interest in the dynamics and control of large space structures (LSS) has spurred a need for a better understanding of truss structure joints. The main function of these joints is to connect one or more truss elements together to form space-frame structures. However, another important function that they serve is to provide passive damping to these flexible space structures.[1,2] It is well known that low levels of passive damping are a major concern of controls designers. The low relative stability of LSS may cause small perturbations to the control scheme, such as observation spillover or plant uncertainty, to result in poor performance or even instability in the closed-loop system.[3,4] Recently, it has been shown (quantitatively) that passive damping not only reduces the tendency for instability in flexible structures, but also lessens the model reduction error caused by mode truncation.[5,6] Thus, joints may be a simple but effective way to ease the stringent requirements on the controls design. From a mathematical perspective, however, the joints are nonlinear elements and hence are difficult to analyze. For this reason, it is difficult to determine analytically or computationally the overall damping contribution from the joints. Experimental determination of truss structural damping is also hampered by the joint nonlinearities.[7] The prestressing of the joints caused by gravity loading in a laboratory environment causes the measured properties to differ from their operational values encountered in a zero-$g$, zero-atmosphere space environment. Also, because of the large size and low natural frequencies of these systems, it is difficult to perform full-size testing, especially if one wishes to place the entire structure in a vacuum in order to simulate a space atmospheric environment.

This paper addresses the mathematical modeling and numerical analysis of a nonlinear sleeve joint. Although the modeling and control of linear flexible structures has received considerable interest, relatively little has been done on the modeling and control of structures with multiple nonlinear joints. Some work, however, is relevant to the present effort. Hertz and Crawley have studied the experimental and analytical determination of damping in nonlinear LSS.[1,2,8,9] In particular, Refs. 1 and 2 develop simple joint models and single harmonic analyses are performed to estimate loss factors. Hertz and Crawley's work serves as a starting point for the present research effort.

Many of the dissipative mechanisms in space structure joints are tied to nonlinear behavior. One of the major dissipative mechanisms in joints is dry (Coulombic) friction. The general problem of analyzing structures with dry friction has received considerable attention. See, for example, Ferri[10] or the references cited therein. It has been shown that dry friction can cause some significantly nonlinear behavior in an otherwise linear structure. Clearances in mechanical systems are another source of nonlinear behavior in large truss structures. These clearances are often present because of imperfections in nominally "snug" joints or because of wear that can take place on an initially snug design. At times, clearances are purposely designed into a joint in order to facilitate deployment or permit relative slip and impact to occur. In fact, this "impact damping" may be an important contributing factor to the overall damping level of the structure.[2] However, clearances introduce so-called "dead zone" nonlinearities and hysteresis into the system. The clearances further complicate the situation since they can cause the structures to behave differently in space than they do on the ground. This is caused by both the presence of oxidation in the ground environment and ground-level gravity fields that cause different operating points to become effective.[7,9]

The outline of the remainder of the paper is as follows. Section II contains the development of the equations of motion for a rigid beam partially inserted into a sleeve joint as shown in Fig. 1. Results obtained through time integration of this model are presented in Sec. III. Some concluding remarks are contained in Sec. IV.

## II. Sleeve Joint Model Development

This section deals with the modeling of a generic sleeve joint. Although many types of truss structure joint designs are currently used, sleeve joints are relatively simple in concept but still retain many of the important characteristics of more complicated joint geometries. (See Refs. 1 and 2 for a description of other commonly used joint types.) A brief outline of the modeling steps follows. For a more detailed development, see Ferri.[11]

The generic sleeve joint consists of a cylindrical outer sleeve that fits around the end of a mating beam or truss member. As previously mentioned, Hertz and Crawley have developed simple models for such types of joints.[1,2] Their model considers only dry friction nonlinearities. Loss factors are calculated assuming simple harmonic motion and taking a one mode approximation for the beam motion. This model is used as the starting point for the present study.

The major characteristics that need to be modeled in order to develop an accurate general-purpose sleeve joint model are the following:

*Dissipative effects*
- Damping caused by dry friction.
- Damping caused by impact.
- Material damping caused by deformation of the joint.

Received July 2, 1987; revision received May 17, 1988. 

*Assistant Professor, The George Woodruff School of Mechanical Engineering. Member AIAA.

*Geometry and elastic effects*

Overall beam/sleeve geometry including possible clearances between the beam and sleeve.

Hardening spring characteristics caused by large deformations of the beam and/or sleeve.

An attempt has been made to account for the possibility of any of the foregoing effects in the joint models. Although, as pointed out in Ref. 9, many of these effects are difficult to quantify, the qualitative effects of each joint characteristic can be studied through parameter variation.

For the purpose of modeling, it is assumed that the sleeve joint is composed of two parts: an outer sleeve that moves with the one beam and an inner cylinder that moves with the other beam. Figure 1 shows a closeup schematic of the sleeve joint model. Six degrees of freedom are identified to describe the planar motion of the sleeve joint system. Note that $y_1$, $x_1$, and $\theta_1$ are the lateral displacement, longitudinal displacement, and rotation of the end of the left-hand beam (beam 1) and $y_2$, $x_2$, and $\theta_2$ represent the corresponding quantities for the right-hand beam (beam 2). These six generalized coordinates fully describe the interaction of the outer sleeve and the inner cylinder. Three coordinate systems can be identified: the $i,j$ coordinate system that remains fixed in inertial space, the $i_1, j_1$ system that is fixed on sleeve 1, and the $i_2, j_2$ system that is fixed on inner cylinder 2. Unit vectors in the longitudinal and transverse beam directions are respectively represented by $i$ and $j$; $\theta$ is defined to be positive in the counterclockwise direction. Kinematic relationships are used to derive expressions for the distances between beam and sleeve contact points and for the relative velocities between the sleeve and the beam, both tangent to and normal to the contact plane.

One of the main reasons for choosing the six generalized coordinates just defined is the ease with which the relative motion of the sleeve and cylinder can be expressed. Another motivation for this choice of coordinates is that it provides a relatively easy way of incorporating the sleeve joint model into a flexible truss system using either the finite-element method or component mode synthesis techniques. The analysis presented next is developed for the simplified case in which the sleeve is fixed in inertial space, and only beam 2 is allowed to move. The equations and methodology can be extended to the case in which both the sleeve and inner cylinder can move.

Figure 2 shows the deflected position of the sleeve (shown with solid lines) together with the undeflected state (shown with dotted lines). It is seen that the distance from point $E$ to side $BC$ can be expressed as

$$\delta_E = \boldsymbol{j}_1 \cdot \boldsymbol{r}_{EB} \tag{1}$$

where $\boldsymbol{r}_{EB}$ is the vector from $B$ to point $E$ as shown in Fig. 2. After describing $\boldsymbol{r}_{EB}$ in terms of sleeve length and deflection parameters, Eq. (1) gives

$$\delta_E = (x_1 - x_2 - L_1)\sin\theta_1 + (y_2 - y_1)\cos\theta_1 + L_2\sin(\theta_1 - \theta_2) - (d_2/2)\cos(\theta_1 - \theta_2) + (d_1/2) \tag{2}$$

Fixing the sleeve in inertial space is accomplished by setting $x_1 = y_1 = \theta_1 = 0$. This yields

$$\delta_E = y_2 - L_2\sin\theta_2 - (d_2/2)\cos\theta_2 + (d_1/2) \tag{3}$$

A similar analysis can be performed to obtain $\delta_F$, defined to be the distance from point $F$ to side $AD$. The distance from point $I$ to side $AB$ is similarly defined as $\delta_I$. The remaining distances are defined along the direction transverse to the beam; $\delta_C$ and $\delta_D$ are defined as the distances from point $C$ to side $EH$ and from point $D$ to side $FG$, respectively. In each case, the distances are defined to be positive when contact is not occurring at that respective point. Complete details and expressions may be found in Ref. 11.

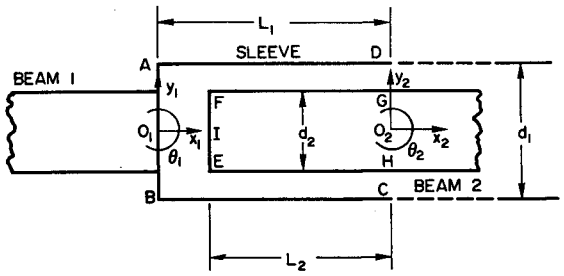


**Fig. 1 Sleeve joint model.**

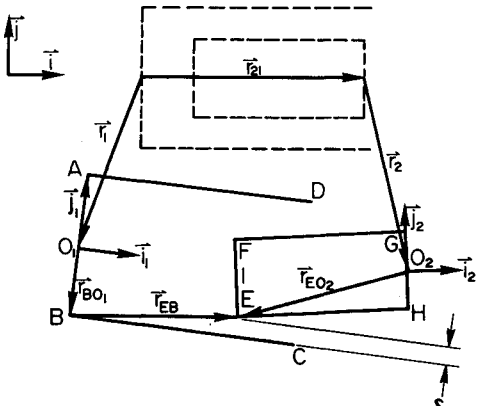


**Fig. 2 Deflected position of sleeve joint.**

In order to model the contact forces, nonlinear, one-way springs are placed at the four contact points. (See Fig. 3.) The term "one-way" implies that the spring forces can be only compressive in nature; no tension is allowed. Mathematically, the spring force at contact point $E$ is given by

$$F_{E_1} = F_{E_1} j; \qquad F_{E_1} = \begin{cases} K_1|\delta_E| + \epsilon_1|\delta_E|^3 & \delta_E \le 0 \\ 0 & \delta_E > 0 \end{cases} \tag{4}$$

where $K_1$ represents the linearized, small deformation elastic constant and $\epsilon_1$ is typically a small, positive quantity that determines the spring "hardening" characteristic at contact points $E$ and $F$. As seen in Fig. 3, parameters $K_2$ and $\epsilon_2$ correspond to stiffness characteristics at contact points $C$ and $D$. For a particular sleeve joint, $K_1$, $K_2$, $\epsilon_1$, and $\epsilon_2$ might be found from a finite-element model or perhaps by approximate methods from the theory of elasticity. Expressions similar to that shown in Eq. (4) can be obtained for the spring forces at contact points $F$, $C$, and $D$. Note that forces $F_{E1}$ and $F_{F1}$ act normal to sides $BC$ and $AD$, respectively, and that forces $F_{D1}$ and $F_{C1}$ act normal to sides $FG$ and $EH$, respectively.

In addition to the four transverse springs already discussed, a linear spring is placed at location $I$ to model the retaining characteristic of the sleeve joint, if any. Only this spring at location $I$ is allowed to transmit both tension and compression.

The total compressive force at locations $E$, $F$, $D$, and $C$ will consist of the elastic force from the springs plus any viscous damping or rate-dependent forces. In order to model the rate-dependent forces caused by material deformation and impact, viscous damping elements are placed in parallel with the one-way nonlinear springs as shown in Fig. 3. Like the springs, the dampers are also permitted to transmit compressive forces only. Thus, the viscous damping forces are nonzero only when contact has occurred ($\delta < 0$) *and* when the relative velocity is such that further compression takes place; that is, $\dot{\delta} < 0$.

The viscous damping forces are proportional to the rate of deflection of the beam or sleeve. These deflection rates can be

found by differentiating the corresponding expressions for $\delta$. For example, the expression for $\dot{\delta}_E$ is

$$\dot{\delta}_E = \dot{y}_2 - L_2\dot{\theta}_2 \cos\theta_2 + (d_2/2)\,\dot{\theta}_2 \sin\theta_2 \tag{5}$$

The corresponding expression for the viscous damping force at point $E$ is given by

$$\boldsymbol{F}_{E_2} = F_{E_2}\boldsymbol{j}; \qquad F_{E_2} = \begin{cases} C_1|\dot{\delta}_E| & \delta_E \le 0, \quad \dot{\delta}_E \le 0 \\ 0 & \text{otherwise} \end{cases} \tag{6}$$

Similar expressions can be found for the other contact points. Whereas the dampers at points $E$, $F$, $C$, and $D$ are one-way in nature, the damper at location $I$ is two-way and is, in fact, a fully linear viscous damper.

The total compressive force at contact point $E$ is found by summing the spring and damper forces:

$$\boldsymbol{F}_E = \boldsymbol{F}_{E_1} + \boldsymbol{F}_{E_2} = F_E\boldsymbol{j} \tag{7}$$

When contact occurs, friction forces come into play, acting tangent to the contact plane. The friction forces can be modeled approximately by Coulomb's Law. In the most general case, two coefficients of friction can be defined: a static coefficient of friction $\mu_s$ that applies when sticking has occurred, and a dynamic or kinetic coefficient of friction $\mu_d$ that applies when slipping occurs. When sticking takes place, the friction force has whatever value it needs to maintain equilibrium at that contact point. If the force required is greater than $\mu_s N$, where $N$ is the normal force to the contact plane, then slipping is said to occur. In the case of slipping, the friction force has magnitude $\mu_d N$ and a direction that opposes the relative movement of the contact plane.

As discussed in the preceding paragraph, the friction forces depend on the signs of the relative slip speeds. Note that the relative slip speed is the component of the relative velocity along the contact plane (or contact line for the planar system under consideration). For contact point $E$, the relative velocity in question is the difference in the absolute velocities of points $E_1$ and $E_2$, where $E_1$ is the point along side $BC$ of the sleeve (body 1) that is in contact with the corner $E_2$ on the inner cylinder (body 2). That is,

$$\boldsymbol{V}_{E_1/E_2} = \boldsymbol{V}_{E_1} - \boldsymbol{V}_{E_2} \tag{8}$$

Since the sleeve is fixed in space, $\boldsymbol{V}_{E_1} = \boldsymbol{0}$. The coordinates $x_2$, $y_2$, and $\theta_2$ can be used to find $\boldsymbol{V}_{E_2}$

$$\boldsymbol{V}_{E_2} = \frac{\mathrm{d}}{\mathrm{d}t}(\boldsymbol{r}_2 + \boldsymbol{r}_{EO_2}) \tag{9}$$

Vectors $\boldsymbol{r}_2$ and $\boldsymbol{r}_{E0_2}$ are seen in Fig. 2 to be given by

$$\boldsymbol{r}_2 = x_2\,\boldsymbol{i} + y_2\,\boldsymbol{j}; \qquad \boldsymbol{r}_{EO_2} = -L_2\,\boldsymbol{i}_2 - (d_2/2)\,\boldsymbol{j}_2$$

Substituting these expressions into Eq. (9) and accounting for the rotation of the unit vectors $\boldsymbol{i}_2$ and $\boldsymbol{j}_2$ gives

$$\boldsymbol{V}_{E_2} = (\dot{x}_2\,\boldsymbol{i} + \dot{y}_2\,\boldsymbol{j}) + \dot{\theta}_2\,\boldsymbol{k}\,x[-L_2\,\boldsymbol{i}_2 - (d_2/2)\,\boldsymbol{j}_2] \tag{10a}$$

$$\boldsymbol{V}_{E_2} = [\dot{x}_2 + (d_2/2)\,\dot{\theta}_2\cos\theta_2 + L_2\dot{\theta}_2\sin\theta_2]\,\boldsymbol{i} + [\dot{y}_2 + (d_2/2)\,\dot{\theta}_2\sin\theta_2 - L_2\dot{\theta}_2\cos\theta_2]\,\boldsymbol{j} \tag{10b}$$

The relative slip speed is the component of the difference in absolute velocities in the direction of the contact plane (side $BC$)

$$V_{E12} = (\boldsymbol{V}_{E_1} - \boldsymbol{V}_{E_2}) \cdot \boldsymbol{i} \tag{11a}$$

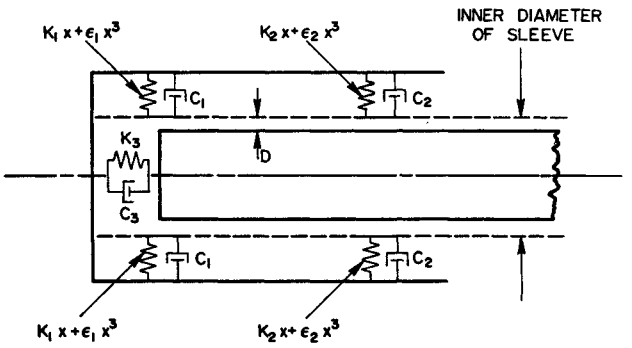


**Fig. 3 Sleeve joint model showing nonlinear, one-way springs and impact dampers ($x$ = compression of the springs).**

$$V_{E12} = -\dot{x}_2 - (d_2/2)\,\dot{\theta}_2\cos\theta_2 - L_2\dot{\theta}_2\sin\theta_2 \tag{11b}$$

Again, similar expressions can be found for the other contact points.

The friction force at point $E$ is determined using the relative slip speed and Coulomb's Law

$$f_E = \begin{cases} f_E\,i, & f_E \le \mu_s F_E \qquad V_{E12} = 0 \\ \mu_d F_E \operatorname{sgn}(V_{E12})\,i & V_{E12} \ne 0 \end{cases} \tag{12}$$

where

$$\operatorname{sgn} V = \begin{cases} 1 & V > 0 \\ 0 & V = 0 \\ -1 & V < 0 \end{cases} \tag{13}$$

The friction forces at contact points $F$, $C$, and $D$ can be found in a similar manner. Note that the contact line (and, hence, the friction forces) at locations $C$ and $D$ are parallel to the sides $EH$ and $FG$, respectively.

### Equations of Motion

The normal forces and friction forces constitute all of the forces exerted on the beam by the sleeve. In addition to the beam-sleeve interaction forces, an externally applied excitation force $\boldsymbol{F}(t) = F(t)\boldsymbol{j}$ acts on the beam as seen in the free-body diagram shown in Fig. 4. The equations of planar motion for this system are obtained from two force balances and one moment balance about the beam's center of gravity (c.g.)

$$m\,\ddot{x}_c = F_x \tag{14}$$

$$m\,\ddot{y}_c = F_y + F(t) \tag{15}$$

$$\begin{aligned} I_C\,\ddot{\theta} = {} & F_F\left(\frac{L_2}{2}\cos\theta + \frac{d_2}{2}\sin\theta\right) + f_F\left(\frac{L_2}{2}\sin\theta - \frac{d_2}{2}\cos\theta\right) \\ & + F_E\left(-\frac{L_2}{2}\cos\theta + \frac{d_2}{2}\sin\theta\right) + f_E\left(\frac{L_2}{2}\sin\theta + \frac{d_2}{2}\cos\theta\right) \\ & + \frac{L_2}{2}F_I\sin\theta - (F_D - F_C)\frac{L_2}{2} - (f_D - f_C)\frac{d_2}{2} \\ & + F_D\,r_{D_2G} - F_C\,r_{C_2H} + L_4\sin\theta\,F_x - L_4\cos\theta\,F_y \\ & + \left(L_F\cos\theta + \frac{d_2}{2}\sin\theta\right)F(t) \end{aligned} \tag{16}$$

where $m$ is the mass of the beam, $I_c$ is the mass moment of inertia about the beam's c.g., $F_x$ and $F_y$ are beam-sleeve

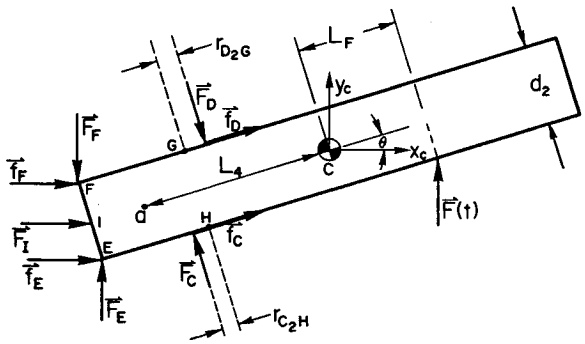


**Fig. 4 Beam free-body diagram.**

interaction forces in the $x$ and $y$ directions, respectively

$$F_x = F_I + f_E + f_F + (F_D - F_C)\sin\theta + (f_D + f_C)\cos\theta \quad (17)$$

$$F_y = F_E - F_F + (F_C - F_D)\cos\theta + (f_D + f_C)\sin\theta \quad (18)$$

and where $r_{D_2G}$ and $r_{C_2H}$ are given by

$$r_{D_2G} = [x_2^2 - x_2 d_2 \sin\theta + (d_2/2)^2 + y_2^2 - y_2(d_1 - d_2\cos\theta) + (d_1/2)^2 - (d_1 d_2/2)\cos\theta]^{1/2} \quad (19)$$

$$r_{C_2H} = [x_2^2 + x_2 d_2 \sin\theta + (d_2/2)^2 + y_2^2 + y_2(d_1 - d_2\cos\theta) + (d_1/2)^2 - (d_1 d_2/2)\cos\theta]^{1/2} \quad (20)$$

Equations (14-16) form the equations of motion for a rigid beam partially inserted into a sleeve joint. Defining the state vector as

$$x = [x_c, y_c, \theta, \dot{x}_c, \dot{y}_c, \dot{\theta}]^T$$

the equations of motion can be summarized in first-order vector form

$$\dot{x} = f[x, F(t)] \quad (21)$$

## III. Results for the Sleeve Joint Model

One of the advantages of the rigid beam fixed-sleeve model developed in Sec. II is that it isolates the sleeve joint so that an accurate assessment of its effects can be made. For example, since the beam is rigid, the total damping of this system is entirely caused by the dry friction and material damping in the joint. Hence, the damping contribution of the joint to the system is easily determined. Another advantage of this model is that it allows one to perform many parametric studies at a relatively low computational cost.

A baseline configuration for the fully nonlinear joint model was chosen to have the parameter values given in Table 1. Length dimension nomenclature is defined in Fig. 5. The coefficient of friction $\mu$ is the baseline value for both the static and dynamic coefficients of friction; that is, $\mu_s = \mu_d = \mu$. Unless otherwise stated, parameters may be assumed to have their baseline value.

A sample time response is shown in Figs. 6 and 7. The quantity $y_2$ refers to the transverse displacement of the beam at a position that lies just outside the sleeve (see Fig. 1). The figures show the free response of $y_2$ and $\theta$ for the baseline set of parameter values and a particular set of initial conditions: $x_2 = 0$, $y_2 = 0.003$ m, $\theta = 0.09$ rad. The plotted quantities are normalized by various system parameters. The displacement $y_2$ is normalized with respect to the clearance $D = (d_1 - d_2)/2$. If $|y_2/D| > 1$, it implies that contact is taking place. The beam rotation $\theta$ is normalized with respect to $D/(L_2/2)$. This is the approximate beam rotation (in radians) when contact begins to occur. Thus, $|\theta \cdot L_2/(2D)| > 1$ also implies that contact has occurred.

The motion shown in Figs. 6 and 7 is largely composed of two frequencies: a highly damped, high-frequency motion ($\sim$24 rad/s) related to transverse displacement of the beam's end, and a dominant low-frequency motion ($\sim$0.4 rad/s at high amplitudes) related to the gross rotation of the beam.

The significance of these two types of motions can be determined by examining the linearized equations of motion for a sleeve joint model with no clearances

$$m\ddot{x}_c + K_x x_c = 0 \quad (22)$$

$$m\ddot{y}_c + K_y y_c - L_4 K_y \theta = 0 \quad (23)$$

**Table 1 Baseline parameter values for sleeve joint model**

| Item | Symbol | Baseline value | Units |
|---|---|---|---|
| Mass | $m$ | 1.3493 | kg |
| Mass moment of inertia | $I_c$ | 0.12167 | kg · m$^2$ |
| Lateral stiffness | $K_1$ | 100 | N/m |
| Lateral stiffness | $K_2$ | 100 | N/m |
| Longitudinal stiffness | $K_3$ | 100 | N/m |
| Cubic stiffness | $\epsilon_1$ | 0 | N/m$^3$ |
| Cubic stiffness | $\epsilon_2$ | 0 | N/m$^3$ |
| Lateral damping | $C_1$ | 0 | N · s/m |
| Lateral damping | $C_2$ | 0 | N · s/m |
| Longitudinal damping | $C_3$ | 0 | N · s/m |
| Coefficient of friction | $\mu$ | 0.47 | – – |
| Sleeve length | $L_1$ | 0.0401 | m |
| Inner cylinder length | $L_2$ | 0.04 | m |
| Distance from c.g. to point 2 | $L_3$ | 0.48 | m |
| Distance from c.g. to point a | $L_4$ | 0.50 | m |
| Distance from c.g. to forcing | $L_F$ | 0 | m |
| Total beam length | $L_{\text{total}}$ | 1.04 | m |
| Inner sleeve diameter | $d_1$ | 0.0252 | m |
| Outer beam diameter | $d_2$ | 0.0250 | m |

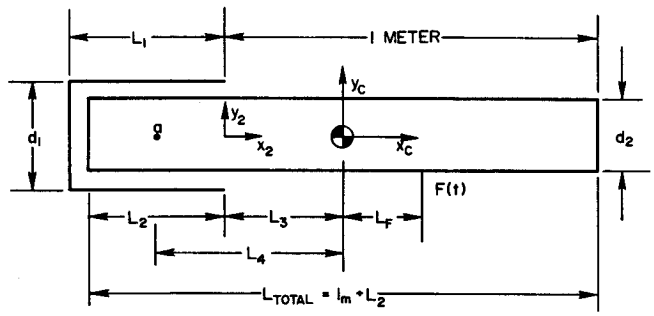


**Fig. 5 Definition of length and displacement parameters.**

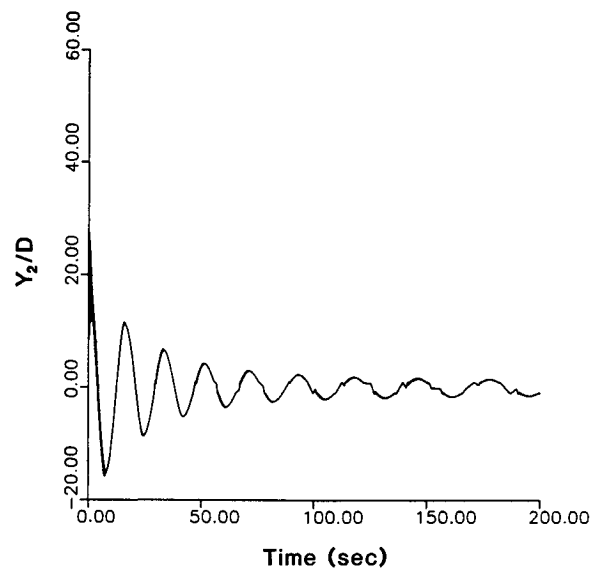


**Fig. 6 $y_2/D$ vs time. Baseline sleeve joint model. Initial conditions $x_2(0) = 0.0$, $y_2(0) = 0.003$ m, $\theta(0) = 0.09$ rad.**

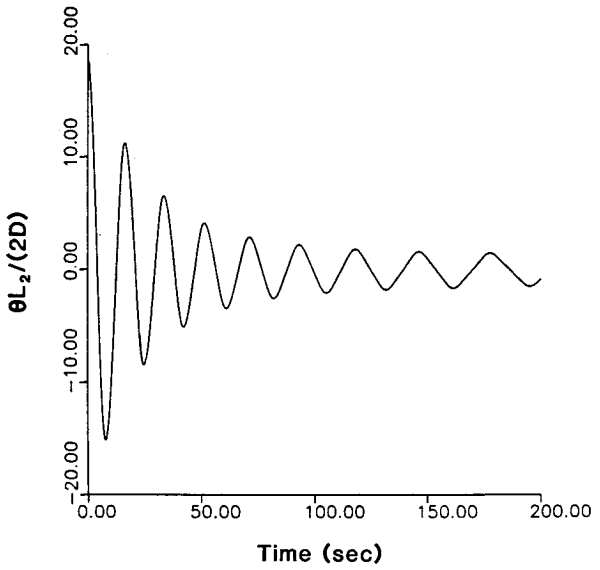


**Fig. 7 $\theta L_2/(2D)$ vs time. Baseline sleeve joint model. Initial conditions $x_2(0) = 0.0$, $y_2(0) = 0.003$ m, $\theta(0) = 0.09$ rad.**

$$I_c\,\ddot{\theta} - K_y L_4 y_c + (K_\theta + K_y L_4^2)\theta = 0 \tag{24}$$

$K_x$, $K_y$, and $K_\theta$ can be defined approximately as follows:

$$K_x = K_3$$

$$K_y = K_1 + K_2$$

$$K_\theta = (L_2^2/4)(K_1 + K_2)$$

Since Eq. (22) is uncoupled from Eqs. (23) and (24), we can easily identify the natural frequency for longitudinal motion to be

$$\omega_1 = \sqrt{K_x/m} = \sqrt{K_3/m} \tag{25}$$

The natural frequencies associated with the remaining two equations are found to be (if we assume $K_1 = K_2$)

$$\omega_{2,3}^2 = K_1\left[\frac{m\,L^2 + 2I_c \pm \sqrt{(mL^2 + 2I_c)^2 - 4m\,I_c\,L_2^2}}{2m\,I_c}\right] \tag{26}$$

where $L^2 \equiv 1/2\,L_2^2 + 2L_4^2$. If we use baseline parameters, this gives

$$\omega_1 = \sqrt{K_3}\,(0.861), \quad \omega_2 = \sqrt{K_1}\,(0.0417), \quad \omega_3 = \sqrt{K_1}\,(2.366) \tag{27}$$

It is seen that the natural frequencies of the system grow as $\sqrt{K}$. More important, the difference between $\omega_3$ and $\omega_2$ also grows with $\sqrt{K_1}$, causing the equations of motion to become numerically "stiff" as the joint gets physically stiffer.[12] Numerical solutions to stiff differential equations require large amounts of computer time in order to maintain accuracy. For this reason, most of the simulations presented here are done for the cases of relatively low joint stiffness, with results for higher stiffnesses based on extrapolation and relatively fewer numerical simulations.

When we examine the eigenvectors associated with Eqs. (23) and (24), it is seen that for the case $K_1 = K_2 = 100$ N/m ($K_y = 200$ N/m), the low-frequency motion corresponds to the case where $y_2$ and $\theta$ are "in phase" and the high-frequency motion corresponds to the case where $y_2$ and $\theta$ are "out of phase." Although the longitudinal degree of freedom does not interact strongly with the other two degrees of freedom, it is very important in accurately predicting the losses caused by friction. Hence, the longitudinal degree of freedom is retained for the subsequent computations, but concentration will be directed to $y_2$ and $\theta$ since these quantities dominate the global motion of the beam.

There are two aspects of Figs. 6 and 7 that are worth noting. The first is that the envelopes of decay are largely exponential. Note that the entire damping of this system is the result of dry friction, since the baseline model has the impact damping parameters set equal to zero ($C_1 = C_2 = C_3 = 0$). In classical dry friction damped systems, the normal forces are independent of amplitude and, consequently, the envelopes of decay are linear.[13] In this case, however, the normal forces at the contact points vary depending on the beam motion; in particular, they are dependent on the compression of the one-way springs. As a result of this amplitude dependence, the envelopes of decay are exponential. This type of behavior has been found in other systems with amplitude-dependent friction as well.[1,14]

A second important observation from Figs. 6 and 7 is that the frequency appears to be strongly affected by the amplitude of response. As the amplitude grows smaller, the frequency of response becomes lower. This can be understood by examining a describing function approximation of the piecewise linear springs of the simplified sleeve joint model. As the amplitude decreases, the effective spring constant also decreases. In fact, for amplitudes of response smaller than the clearance displacement, the effective spring constant is zero.

The damping ratio for the low-frequency motion was estimated using the log decrement approach. The formula for the damping ratio, provided that $\zeta << 1$, is[13]

$$\zeta \simeq (1/2\pi)\,\delta = (1/2\pi)\,\ell n\,(\xi_1/\xi_2) \tag{28}$$

where $\xi_1$ is the amplitude of one peak in a free response and $\xi_2$ is the amplitude of the next peak. It should be noted that the log decrement approach is derived for single-degree-of-freedom (single-DOF) linear systems; thus, it is only an approximate formula when applied to nonlinear, multi-DOF systems. From Fig. 6, we see that initially, when $y_2/D = 30$, the damping ratio is approximately $\zeta = 0.146$. After the amplitude decreases, $y_2/D = 12$, the damping ratio is reduced to $\zeta = 0.079$. Thus, it is seen that, qualitatively, low-amplitude motions are more lightly damped than high-amplitude motions. This characteristic was seen in many of the results of this research.

The effect of beam sleeve geometry on overall damping is shown in Fig. 8 for a stiffness of $K_1 = K_2 = K_3 = 10$ N/m. The quantity $D/L_2$ is essentially a relative clearance defined as the true clearance, $D = (d_1 - d_2)/2$, divided by the sleeve length $L_2$. It is seen that the damping ratio is inversely proportional to $D/L_2$; that is, small clearances are more beneficial for dry friction damping than large clearances. Note that the abscissa of the graph is the (unnormalized) amplitude of $y_2$. (This quantity is left unnormalized because the clearance $D$ is being varied from curve to curve.) It is also seen that for a given $D/L_2$, the damping ratio increases with amplitude.

The effects of sleeve joint stiffness and coefficient of friction were also studied. Damping ratios were computed for joint stiffness values ranging from $K_1 = K_2 = K_3 = 0.1$ N/m to $10 \times 10^6$ N/m. It was found that, even over such a broad range of values, the system damping ratio was relatively insensitive to changes in joint stiffness. Of course, increasing the sleeve stiffness increases system natural frequencies so that the response decays to zero faster, but it undergoes the same number of oscillations before it settles out. A variation of the coefficient of friction between 0 and 1.0 revealed that $\mu$ affects the damping ratio in a linear manner.

The baseline system was forced with a sinusoidal point force to generate frequency-response information. The forcing is assumed to be applied to the center of mass of the beam; that is, $L_F = 0$. A normalization for the forcing amplitude was chosen to be $F_n = K_y D L_2/(2L_4)$ where $K_y = K_1 + K_2$. It may be

noted that this is the static force necessary to deflect the beam through an angle of $2D/L_2$ rad. Using baseline parameters, $F_n$ is $8 \times 10^{-4}$ N. The frequency-response curves for $F/F_n = 3$, 3/2, and 3/16 are shown in Fig. 9. The amplitude shown is the peak response per cycle. Observations of the time histories of the forced response revealed that the motion was often multiharmonic in nature. At low frequencies, the motion typically had a third or fifth harmonic of the forcing frequency significantly present. An example of such superharmonic response is shown in Fig. 10 for a forcing frequency of $\omega = 0.1$ rad/s and forcing level $F/F_n = 3$. At or near resonance, the motion was mainly sinusoidal in nature. However, at higher frequencies, subharmonic response was typical. Figure 11 shows the response for $\omega = 1.0$ rad/s and $F/F_n = 3$. It is seen that the motion is dominated by a 1/5 subharmonic response; that is, the motion repeats after every five cycles of the forcing. Such types of motion were typical at the higher frequencies at each of the three force levels investigated. Often, very low-order subharmonics were observed (on the order of 1/20th) or even at times aperiodic beating motion, which indicated the presence of two or more noncommensurable frequencies of response.[15] It should be added that such unusual behavior is not uncommon for nonlinear systems and, in particular, for systems with clearances. See, for example, the papers by Shaw and Holmes,[16,17] which examine the existence of chaos in mechanical systems with clearances.

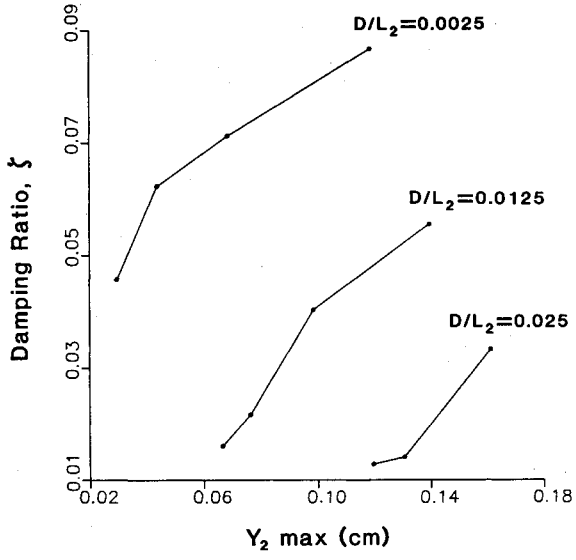


Fig. 8 Damping ratio vs peak displacement $y_2$ in centimeters; various values of $D/L_2$.

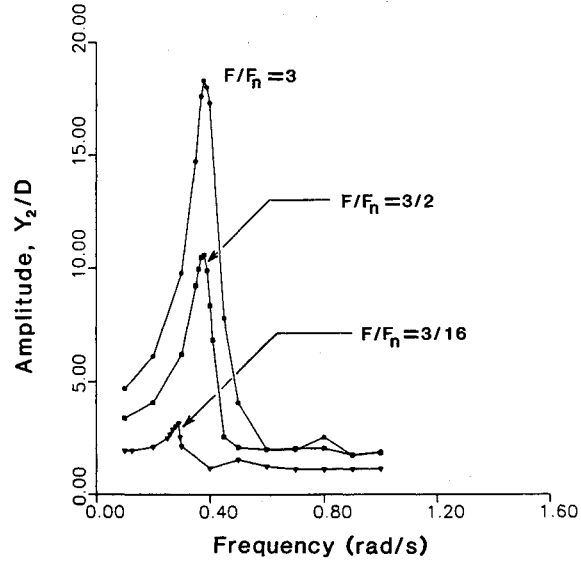


Fig. 9 Amplitude $y_2/D$ vs frequency of excitation; various levels of excitation amplitude (baseline sleeve joint model).

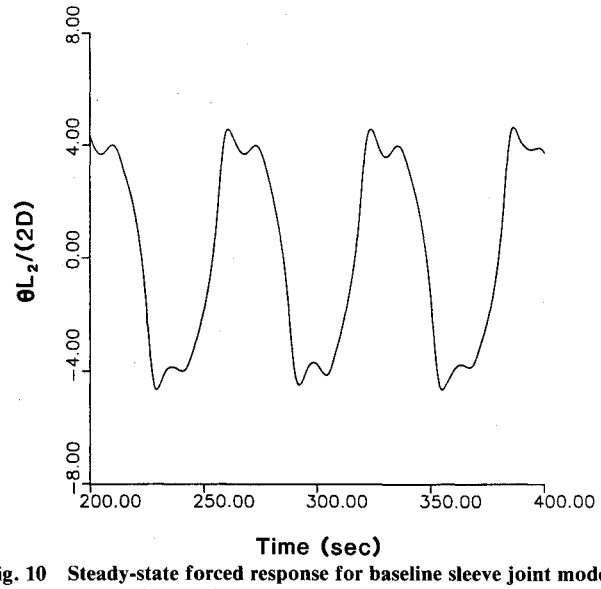


Fig. 10 Steady-state forced response for baseline sleeve joint model. $F/F_n = 3.0$, $\omega = 0.1$ rad/s.

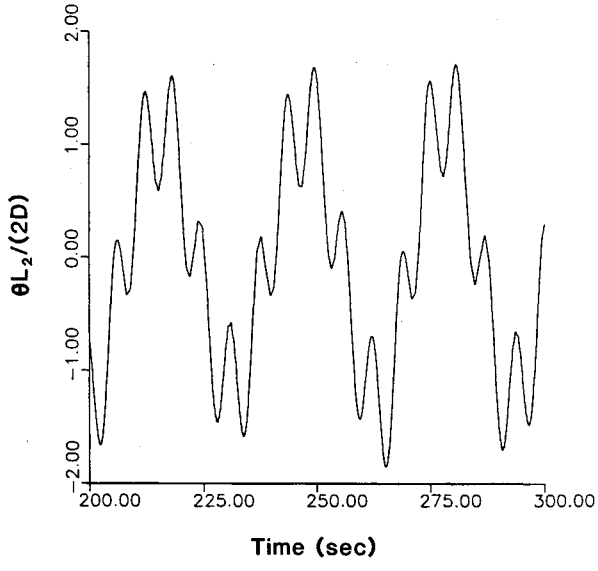


Fig. 11 Steady-state forced response for baseline sleeve joint model. $F/F_n = 3.0$, $\omega = 1.0$ rad/s.

## IV. Concluding Remarks

A generic sleeve joint model has been developed that accounts for clearances, geometric stiffening, dry friction, and impact damping. This model was then tested using numerical integration to determine the damping contribution from the joint and the overall dynamic behavior of the beam-sleeve system. A parametric study was conducted to determine the qualitative influence of various joint characteristics on the damping contribution of the joint. It was found that the overall damping was qualitatively similar to viscous damping, even for the case of zero impact damping. It was also seen that the system damping ratio was dependent on the amplitude of response; high-amplitude motions had greater damping than low-amplitude motions. Forced response to harmonic excitation revealed noticeable hardening spring behavior. In addition, the time response to harmonic excitation displayed both subharmonic and superharmonic response.

## Acknowledgment

This work was supported by Honeywell, Inc., Space and Strategic Avionics Division and, partially, by National Science Foundation Grant MSM-8707846. Dr. John F. L. Lee and Dr. Elbert Marsh were the respective technical monitors.

## References

[1]Hertz, T. J. and Crawley, E. F., "Damping in Space Structure Joints," AIAA Paper 84-1039, May 1984.

[2]Hertz, T. J. and Crawley, E. F., "The Effects of Scale on the Dynamics of Flexible Space Structures," Space Systems Lab., Dept. of Aeronautics and Astronautics, MIT, Rept. SSL 18-83, Cambridge, MA, Sept. 1983.

[3]Balas, M. J., "Active Control of Flexible Systems," *Journal of Optimization Theory and Applications*, Vol. 25, July 1978, pp. 415–436.

[4]Nurre, G. S., Ryan, R. S., Scofield, H. N., and Sims, J. L., "Dynamics and Control of Large Space Structures," *Journal of Guidance, Control, and Dynamics*, Vol. 7, Sept.-Oct. 1984, pp. 514–526.

[5]Alberts, T. E., Hastings, G. G., Book, W. J., and Dickerson, S. L., "Experiments in Optimal Control of a Flexible Arm with Passive Damping," *Proceedings of the 5th VPI & SU/AIAA Symposium on Dynamics and Control of Large Structures*, AIAA New York, June 1985, pp. 423–435.

[6]Alberts, T. E., "Augmenting the Control of a Flexible Manipulator with Passive Mechanical Damping," Ph.D. Thesis, School of Mechanical Engineering, Georgia Inst. of Technology, Atlanta, GA, Sept. 1986.

[7]Hanks, B. R. and Pinson, L. D., "Large Space Structures Raise Testing Challenges," *Astronautics and Aeronautics*, Vol. 21, Oct. 1983, pp. 34–40.

[8]Crawley, E. F., Sarver, G. L., and Mohr, D. G., "Experimental Measurement of Passive Material and Structural Damping for Flexible Space Structures," *Acta Astronautica*, Vol. 10, May–June 1983, pp. 381–393.

[9]Crawley, E. F. and Aubert, A. C., "Identification of Nonlinear Structural Elements by Force-State Mapping," *AIAA Journal*, Vol. 24, Jan. 1986, pp. 155–162.

[10]Ferri, A. A., "The Dynamics of Dry Friction Damped Systems," Ph.D. Thesis, Dept. of Mechanical and Aerospace Engineering, Princeton Univ., Princeton, NJ, Sept. 1985.

[11]Ferri, A. A., "The Influence of Nonlinear Joints on the Dynamics of Large Flexible Space Structures," Honeywell, Inc., Space and Strategic Avionics Division, Clearwater, FL, Final Rept. April 1987.

[12]Gear, C. W., *Numerical Initial Value Problems in Ordinary Differential Equations*, Prentice-Hall, Englewood Cliffs, NJ, 1971.

[13]Meirovitch, L., *Elements of Vibration Analysis*, McGraw-Hill, New York, 1975.

[14]Bielawa, R. L., "An Analytic Study of the Energy Dissipation of Turbomachines Bladed-Disk Assemblies Due to Inter-Shroud Segment Rubbing," *Journal of Mechanical Design, Transaction of ASME*, Vol. 100, April 1978, pp. 222–228.

[15]Hayashi, C., *Nonlinear Oscillations in Physical Systems*, McGraw-Hill, New York, 1964.

[16]Shaw, S. W. and Holmes, P. J., "A Periodically Forced Piece-Wise Linear Oscillator," *Journal of Sound and Vibration*, Vol. 90, Sept. 1983, pp. 129–155.

[17]Shaw, S. W. and Holmes, P. J., "A Periodically Forced Impact Oscillator with Large Dissipation," *ASME Journal of Applied Mechanics*, Vol. 50, Dec. 1983, pp. 849–857.